INFORMATION TO USERS

This manuscript has been reproduced from the microfilm master. UMI films the text directly from the original or copy submitted. Thus, some thesis and dissertation copies are in typewriter face, while others may be from any type of computer printer.

The quality of this reproduction is dependent upon the quality of the copy submitted. Broken or indistinct print, colored or poor quality illustrations and photographs, print bleedthrough, substandard margins, and improper alignment can adversely affect reproduction.

In the unlikely event that the author did not send UMI a complete manuscript and there are missing pages, these will be noted. Also, if unauthorized copyright material had to be removed, a note will indicate the deletion.

Oversize materials (e.g., maps, drawings, charts) are reproduced by sectioning the original, beginning at the upper left-hand corner and continuing from left to right in equal sections with small overlaps. Each original is also photographed in one exposure and is included in reduced form at the back of the book.

Photographs included in the original manuscript have been reproduced xerographically in this copy. Higher quality 6" x 9" black and white photographic prints are available for any photographs or illustrations appearing in this copy for an additional charge. Contact UMI directly to order.

UMI

A Bell & Howell Information Company
300 North Zeeb Road, Ann Arbor MI 48106-1346 USA
313/761-4700 800/521-0600

VENUS EJECTA PARABOLAS:
COMPARING THEORY WITH OBSERVATION

by

Christian James Schaller

A Thesis Submitted to the Faculty of the

DEPARTMENT OF PLANETARY SCIENCES

In Partial Fulfillment of the Requirements
For the Degree of

MASTER OF SCIENCES

In the Graduate College

THE UNIVERSITY OF ARIZONA

1998

UMI Number: 1389291

UMI Microform 1389291
Copyright 1998, by UMI Company. All rights reserved.

This microform edition is protected against unauthorized copying under Title 17, United States Code.

UMI
300 North Zeeb Road
Ann Arbor, MI 48103

STATEMENT BY AUTHOR

This thesis has been submitted in partial fulfillment of requirements for an advanced degree at The University of Arizona and is deposited in the University Library to be made available to borrowers under rules of the Library

Brief quotations from this thesis are allowable without special permission, provided that accurate acknowledgement of source is made. Requests for permission for extended quotation from or reproduction of this manuscript in whole or in part may be granted by the head of the major department or the Dean of the Graduate College when in his or her judgement the proposed use of the material is in the interests of scholorship. In all other instances, however, permission must be obtained from the author.

SIGNED: _____

APPROVAL BY THESIS DIRECTOR

This thesis has been approved on the date shown below:

Richard Greenberg — April 30, 1998

Richard Greenberg
Professor of Planetary Sciences

Date

ACKNOWLEDGEMENTS

I'd like to thank Jay Melosh and Rick Greenberg for their generous help and encouragement with this project. I also thank Ron Vervack, who developed the model of parabola formation with Jay Melosh.

Thanks also to my officemates over the years, including Bob Reid, Jon Pedicino, David Trilling, and Rachel Mastrapa, for putting up with me. I also thank the people of the Image Processing for Teaching project for the same reason. Kim Cyr and Jennifer Grier also dealt well with my antics. Thanks!

Finally, I must thank the members of Fugitive Group C—'Lon Chaney' Gibbard, 'Fujiwara' Rivkin, 'Isa' Turtle, 'LeMorte' Reid, 'Yewshoot' Coker, 'Lady Kathryn' Mastrapa, 'Sparks' Vervack, and, of course, the Insidious Robotic Wu Han—for numerous nights spent battling the forces of evil, and Doug Dawson for providing us with plenty of surprises along the way.

DEDICATION

To Barbara and Robin Schaller

TABLE OF CONTENTS

ABSTRACT 8

CHAPTER 1. INTRODUCTION AND BACKGROUND 9

CHAPTER 2. THE PARABOLA FORMATION MODEL 14

2.1. Ejecta Transport 14

2.1.1. Phase 1: Ejection into space 14

2.1.2. Phase 2: Ballistic trajectory above the atmosphere 15

2.1.3. Phase 3: Atmospheric re-entry 16

2.1.4. Phase 4: Wind transport 16

2.1.5. Phase 5: Ground deposition 17

2.2. Model Parameters 17

2.3. Method 19

CHAPTER 3. RESULTS 27

CHAPTER 4. DISCUSSION 39

4.1. Source Crater Transition Radius 39

4.2. Agreement with Chicxulub and Extension to Non-Venusian Craters 40

4.3. The Role of Minimum Thickness d 40

CHAPTER 5. CONCLUSIONS 44

REFERENCES 45

LIST OF FIGURES

FIGURE 1a, Parabola Bassi 12

FIGURE 1b, Parabola Bassi (Modeled) 13

FIGURE 2, Wind Transport Distance *vs.* Ejecta Particle Diameter 22

FIGURE 3, Anatomy of a Parabola 23

FIGURE 4, Unnamed Parabola at –39.10°N, 97.10°E 34

FIGURE 5a, DuChatelet Parabola 35

FIGURE 5b, DuChatelet Parabola (Modeled) 36

FIGURE 6, α *vs.* r_c 37

FIGURE 7, d_c *vs.* r_c 38

LIST OF TABLES

TABLE 1, Terminal Speed Altitude *vs.* Particle Size 21

TABLE 2, Observed Parabola Parameters 24

TABLE 3, Modeled Parabola Parameters 31

ABSTRACT

The Magellan radar imager detected approximately 60 dark (i.e. low backscatter cross section) parabola-shaped features on the surface of Venus; each parabola is oriented with the open end toward the west and envelopes an impact crater near its "focus." In this thesis, I use a model of parabola formation to fit the 58 Venusian parabolas observed to date, as well as 9 circular features that are similar to the parabolas; I achieve good results for ~65% of the 41 parabolas that meet the conditions for the model to apply. As a result of modeling the parabolas, I derive a quantitative description of the distribution of small (~1 cm to ~1 μm in diameter) impact ejecta over a planetary surface. My results agree well with the distribution of fine impact ejecta derived for the Terrestrial impact crater Chicxulub. In addition, these results lead to a method for estimating the quantity of fine-grained material available on Venus for surface transport processes such as saltation.

CHAPTER 1

Introduction and Background

During its extended mission to Venus, the Magellan synthetic aperture radar (SAR) detected approximately 60 dark (i.e. low backscatter cross section), parabolic features ("parabolas") in the plains regions of Venus (Campbell et al., 1992). These features share several common characteristics: Each parabola is very large, covering several hundreds of thousands of square kilometers. Each parabola is oriented with the blunt tip (the "head") pointed due east and the open end (the "tail") due west. Finally, each parabola has a crater located on the axis of symmetry, near the blunt, eastern end; in most cases, the crater's floor is bright in radar backscatter cross section. In this thesis, I name each parabola according to the interior, on-axis crater; e.g. Adivar parabola lies around the crater Adivar. Figure 1a shows Bassi, a typical parabola.

In addition to the parabolas, Campbell et al. (1992) report the existence of nine large circular features that resemble the parabolas in every respect other than shape. I include these features in my work here; for convenience, I refer to these circular features as parabolas as well, except where explicitly noted.

The parabolas are most sharply defined and typically exhibit the lowest levels of backscatter cross section (and thus appear darkest) near the head; along the sides and tail, the backscatter cross section blends in with the surrounding plains' backscatter cross section. In most cases, surrounding geological units are visible within the body of the parabola. In a few cases (e.g. Stuart), large geological features actually define the western edge of the parabola's tail, presumably due to the location of the crater in relation to the interrupting feature; in Stuart's case, the interrupting feature is Alpha Regio.

Under the Magellan viewing conditions (i.e. incidence angles between ~15° and ~45°

with a 12.6 cm wavelength radar signal), a low backscatter cross section (a visually dark pixel) implies a smooth surface on scales comparable to the radar wavelength. The location of the craters and the fact that every parabola has a crater suggest that the parabolas are products of impact cratering. The orientation of the parabolas, the generally low backscatter cross section, and the blending of the parabola material with the surrounding plains units suggest that the parabolas formed when the impact crater ejecta scattered under the influence of the high-altitude Venusian winds, which blow from east to west at high speeds.

In cases where the parabolas partially overlap multiple geological units, the stratigraphy implies that the parabolas are among the youngest features on Venus. Based on such stratigraphy, Campbell et al. (1992) suggested that the bright-floored putative source craters are among the freshest, most pristine craters on Venus. Therefore, dark-floored craters are older. Based on crater counts and the observation that ~10% of Venusian craters have parabolas (or extensive circular features similar to parabolas), Arvidson et al. (1992) estimate the mean time to completely erode a parabola to be ~60 million years.

Models of crater ejecta distribution (e.g. McGetchin et al., 1973) have generally focused on the impact ejecta near the crater rim (the proximal ejecta). Particles in this ejecta are typically several centimeters to meters in scale. The parabola particles are probably smaller than that; based on a surface roughness model, Campbell et al. (1992) show that the particles are < 2 cm in diameter.

Vervack and Melosh (1992) investigated the emplacement of this fine, far-flung ("distal") component. Here, I use their model to fit the parameters of the observed Venusian parabolas and derive a quantitative description of fine, distal ejecta distributed over a planetary surface. I thus test the Vervack and Melosh model by investigating how

well, with plausible parameter values, it fits the actual distribution of wind-scattered ejecta fines.

FIGURE 1a. Parabola Bassi

FIGURE 1: (a) The ejecta parabola around the crater Bassi, located at 19.0°S, 64.7°N, r =16.5 km. The entire image is approximately 1800 km across. (Image from C2-MIDR.30S078;1, 201, and 301.)

FIGURE 1b, Parabola Bassi (Modeled)

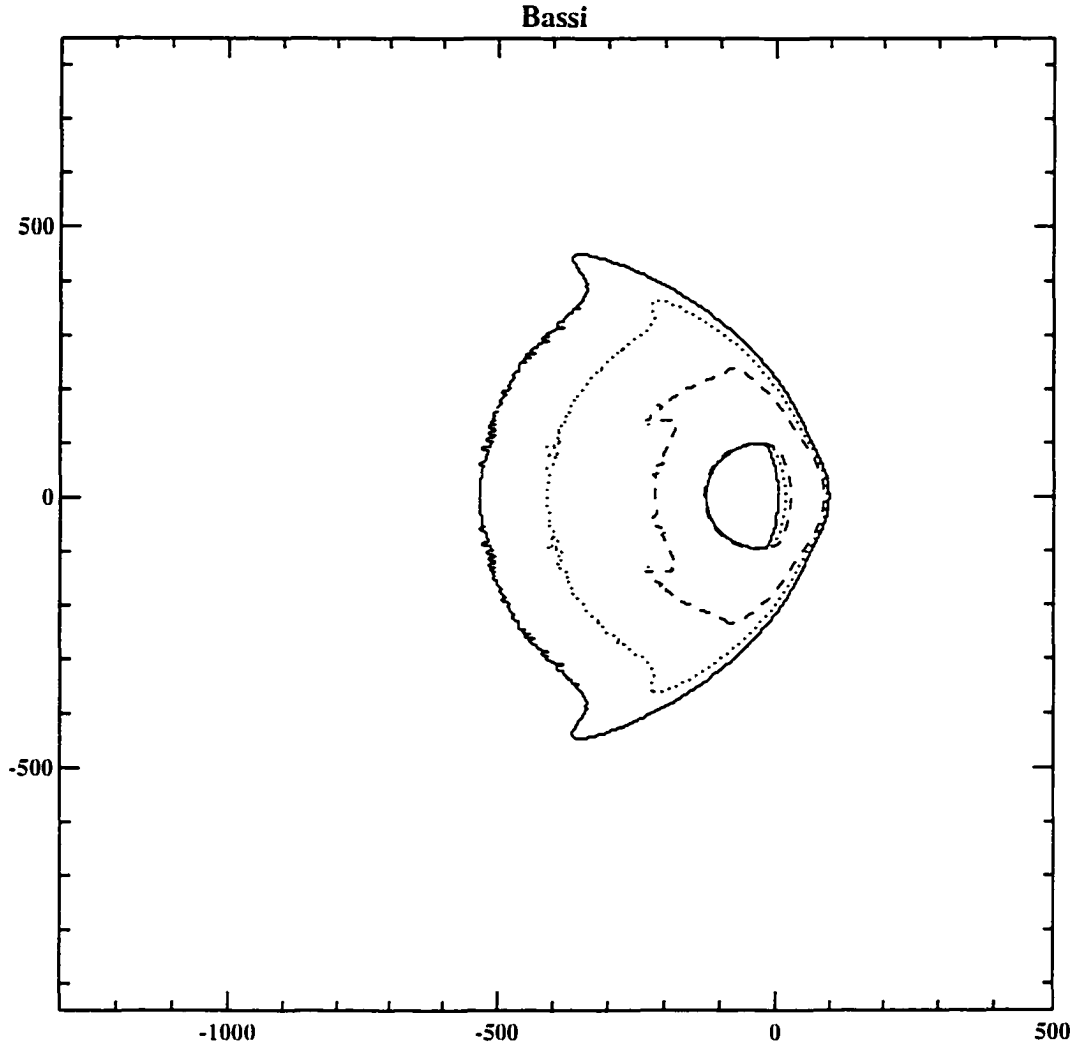

FIGURE 1: (b) Thickness contours for the best fit model of Bassi, using $\alpha = 2.65$. d_c = 12 m, and $\delta = 1$ cm. Contours are shown for 1 cm (solid line), 3 cm (short dash), and 10 cm (long dash). Higher contours were omitted for clarity. Distances are in km. The plot is at the same scale as (a), and the crater Bassi is located at the origin of the plot. The origin of the plot matches the center of Bassi in Fig. 1a.

CHAPTER 2

The Parabola Formation Model

2.1. Ejecta Transport

The Vervack and Melosh model describes a process for transport of ejecta from a crater site to the ejecta's landing point. It consists of five distinct phases: (1) During the formation of the impact crater, the expanding vapor plume carries particles (melt droplets and/or lithic fragments) out of the atmosphere. (2) The particles travel on ballistic trajectories in the vacuum of space. (3) At considerable distances from the source crater, the particles re-enter the atmosphere and rapidly decelerate, after which (4) wind transport is the dominant mechanism. (5) Finally, the particles reach the ground, building up the parabolic shapes observed with the Magellan radar. I briefly review these phases below in order to examine their restrictions and implications in the formation of the parabolas.

2.1.1. Phase 1: Ejection into space

During the formation of the crater, the expanding vapor plume carries particles vertically through the atmosphere. If the crater-forming impact is sufficiently energetic, the plume will expand beyond the atmosphere of the planet. As it rapidly expands into space, the ejecta particles decouple from the vapor, acquiring the ballistic trajectories that carry them the requisite distances. If, however, the energy is insufficient, the plume will not escape the atmosphere, preventing the particles from being widely dispersed.

Vervack and Melosh (1992) showed that the minimum energy required for an atmosphere-breaching plume corresponds to an 8 kilometer radius crater. Thus, the nominal Vervack and Melosh model does not apply for the ~20% of parabolas with

source craters smaller than 8 km in radius. However, that model explicitly neglected aero-braking of projectiles, so the true transition crater radius, r_t, may be larger than 8 km, in which case >20% of parabola-associated craters would not launch ejecta into the second phase. I show in Chapter 3 that the model actually seems to fail for craters of radius $r_c \leq 9.5$ km, so that ~30% of parabolas do not meet the conditions for the model to apply.

2.1.2. Phase 2: Ballistic trajectory above the atmosphere

The exact relationship between a particle's ejection speed (and hence range r) and the particle's diameter d is not precisely known. However, observations of terrestrial tektite and microtektite strewn fields (e.g. Glass and Pizzuto, 1994), as well as analysis of ejecta from the terrestrial impact crater near Chicxulub (Vervack and Melosh, 1992), suggest that smaller particles generally travel greater distances. A general function of the form $r \propto 1/d^{\gamma}$ describes a wide range of possible relationships. Vervack and Melosh (1992) use the following equation to describe a particle's range as a function of its diameter:

$$r = r_c \left(\frac{d_c}{d} \right)^{1/\alpha} \tag{1}$$

In Eq. 1, r_c is the crater radius and d_c (called the "reference particle size") and α are parameters to be determined observationally. Note that the reference size might not represent any real particle, since it is determined by extrapolation to the crater rim; d_c is never measured directly, and the actual particle size on the rim may be different if the extrapolation breaks down at small r. Since smaller particles travel greater distances, I assume α is positive.

2.1.3. Phase 3: Atmospheric re-entry

Particles re-enter the atmosphere with initial speeds and angles determined by their ballistic trajectories. The dense atmosphere decelerates these particles to a terminal speed v_0 at an altitude of z_0. v_0 and z_0 are theoretically-derived functions of the particle size that Vervack and Melosh (1992) have summarized in their Table I; I repeat it here (Table 1) for convenience. In general, smaller particles (with their higher ratio of cross-sectional area to mass) reach terminal speed at higher altitudes than larger particles. I assume that the particles' initial horizontal positions are only negligibly changed during this phase, because the horizontal component of velocity is rapidly reduced to zero for a broad range of particle sizes and entry velocities.

2.1.4. Phase 4: Wind transport

As a particle reaches its terminal speed, wind transport becomes the dominant mechanism for subsequent motion. In this model, I treat an individual particle as a spherical object falling within a dense, moving, fluid atmosphere. Density, viscosity, and wind speed functions of altitude describe this atmosphere; these functions come from the "standard" Venus model atmosphere of Seiff et al. (1985). As described in Chapter 1, it is generally thought that the parabolas are among the youngest Venusian surface features. I assume that changes in the atmosphere since their formation have been negligible, as Seiff et al. have suggested, and that the standard model atmosphere for the present adequately represents the atmosphere at the time the parabolas were formed.

The atmosphere drags a falling particle along with it in the direction of the wind, which is from east to west on Venus. I assume that inter-particle forces produce negligible effects, although Vervack and Melosh (1992) point out that this assumption may be incorrect for large craters. For a given atmospheric profile (wind velocity, etc.),

the resulting horizontal travel distance due to wind transport is a function of particle size and initial altitude, which itself is a function of particle size; I illustrate this function in Figure 2.

2.1.5. Phase 5: Ground deposition

Given that the horizontal offset of a falling particle is a function only of its size and the atmospheric wind profile, and given the assumption that particles of a particular size re-enter the atmosphere at a uniform radial distance from the center of the source crater, one can view the fallen ejecta as a series of offset annuli. Each annulus has a mean radius of r for a given mean particle size, d (Eq. 1). If the particle diameters are sufficiently small ($\leq$ 1 cm, Campbell et al. [1992]), the resulting deposit of material will present a smooth surface to the Magellan radar. Such a surface returns very little backscatter to the radar at Magellan cycle 1 incidence angles, resulting in a "dark" area in the SAR image. If the deposit is sufficiently thick, it will obscure underlying surface features.

2.2. Model Parameters

In this thesis, I consider each of the 57 parabolas and 9 circular features described by Campbell et al. (1992) plus an additional parabola (Winema) not included in that data set. A set of five parameters defines the size and shape of each parabola (Figure 3): the radius of the source crater (r_c), the maximum width W_{max} of the parabola, the parabola's total length L_T, the width W_c of the parabola at the source crater's central longitude, and the distance L_c from the center of the crater to the eastern, blunt tip of the parabola. I list these parameters in Table 2 for the 67 features under consideration. In addition, I list the coordinates of the putative source crater for each parabola. The crater radii and coordinates are from Schaber et al. (1992); W_{max}, L_T, and L_c are from Campbell et al.

(1992). Values for W_c come from my measurements.

A final observational parameter is the thickness of the deposit represented. The existence of an observable parabola requires some minimum thickness δ. Campbell et al. (1992) note that a deposit's thickness must be a significant fraction of a radar wavelength in the medium in order to produce a dielectric interface; they suggest a value of $\sim \lambda / 4\sqrt{\varepsilon}$, or about 2 cm for a Magellan sar $\lambda = 12.6$ and a deposit with dielectric constant $\varepsilon = 3$. They further note that, in order to completely obscure the underlying terrain, δ must be at least comparable to that terrain's surface roughness.

Since the exact value for δ is unknown, I treat it as a free parameter. Those parts of a parabola that are $\leq \delta$ thick are effectively transparent to the Magellan SAR and reveal instead the rocky surface underneath. My measurements and those of Campbell et al. (1992) of the observed parabolas' dimensions represent only that part of the deposit with thickness $\geq \delta$. The theoretical model of Vervack and Melosh (1992) gives deposit thickness as a function of position relative to the crater's center, with the minimum deposit thickness a function of the smallest particle size that re-enters the atmosphere, generally less than δ. In measuring the model parabolas, I cut off the extent of the deposit at the contour level corresponding to thickness δ. This process mainly affects L_T and W_{max}, since the thickness contours are close together at the blunt head of the parabola and are widely dispersed only in the downwind tail.

For a particular crater of radius r_c, the only unknown parameters controlling the model of parabola emplacement are α and d_c in Eq. 1. In what follows, I adjust the parameters α and d_c to fit the observed character and dimensions of Venusian parabolas. The value of δ determines the thickness of the deposit at which I measure L_c, W_c, L_T and W_{max} for a particular model of r_c, α, and d_c.

2.3. Method

In modeling the 67 parabolas under consideration, I followed only those ejecta particles that re-entered the Venusian atmosphere within the range $r_{min} \leq r \leq (0.55\ W_{max})$, where r is the initial horizontal distance from the center of the crater, from Eq. 1. The parameter r_{min} represents the minimum distance beyond which ballistic ejecta fall, since the dense Venusian atmosphere halts ejecta particles that do not initially rise above some minimum height to escape atmospheric drag. Vervack and Melosh (1992) suggest 100 km as a reasonable value for r_{min}; for parabolas with source craters with $r_c \leq 10$ km, I set r_{min} to 50 km in order to account for their smaller sizes. The maximum horizontal distance that the detectible crater ejecta are thrown is $W_{max}/2$, but to account for uncertainty in this measurement, I chose 0.55 W_{max} as the upper limit for my calculations.

To determine the best-fit model parameters α, d_c, and δ for a given parabola, I applied an iterative bisection algorithm to the results of a series of initial models. For each parabola, the initial values of the parameters in Eq. 1 were 2.5, 2.6, and 2.7 for α, and 10 m, 30 m, and 100 m for d_c, based on the work of Vervack and Melosh (1992). I computed the deposit pattern for each of the nine combinations of parameters, and then I measured the deposits' dimensions at $\delta = 1$ cm, $\delta = 3$ cm, and $\delta = 10$ cm. For the next iteration, I set the extreme values of the new range equal to the two values of α and of d_c that yielded a modeled deposit with dimensions L_c, W_c, L_T, and W_{max} that best matched the observed dimensions; the middle value of α and d_c was the average of the two extremes. In general, for a given iteration, I found the best match to each observed dimension in the same region of (α, d_c) parameter space, so that if $\alpha = 2.6$ and $d_c = 1$ m resulted in the best fit to W_c and L_c, the best fit for W_{max} and L_T would have the same (or nearly the same) values for α and d_c. To distinguish between close results, I weighted W_c and L_c more heavily than W_{max} and L_T, because the latter dimensions contain more observational

uncertainty.

I iterated this process until I found an (α, d_c) pair that yielded the best match in all four observed dimensions; I define this pair as the best-fit model. A typical parabola required five to seven iterations to yield the best fit. For most of the observed parabolas, I found the best-fit model at a single value of δ, which was usually either 1 cm or 3 cm. (Cotton and Edinger stand out with $\delta = 50$ cm and 23 cm, respectively.) For Austen, however, I found a good fit at $\delta = 2$ cm as well as at 1 cm, and for Adivar, I found an entire range of δ (from 3 cm to 7 cm) that yielded reasonable modeled deposits.

TABLE 1, Terminal Speed Altitude *vs.* Particle Size

Particle Diameter (cm)	Altitude (km)
10	53
1	67
0.1	78
0.01	87
0.001	96

TABLE 1: Altitude below which ballistic ejecta particles fall at terminal speed on Venus. From Vervack and Melosh (1992).

FIGURE 2. Wind Transport Distance *vs.* Ejecta Particle Diameter

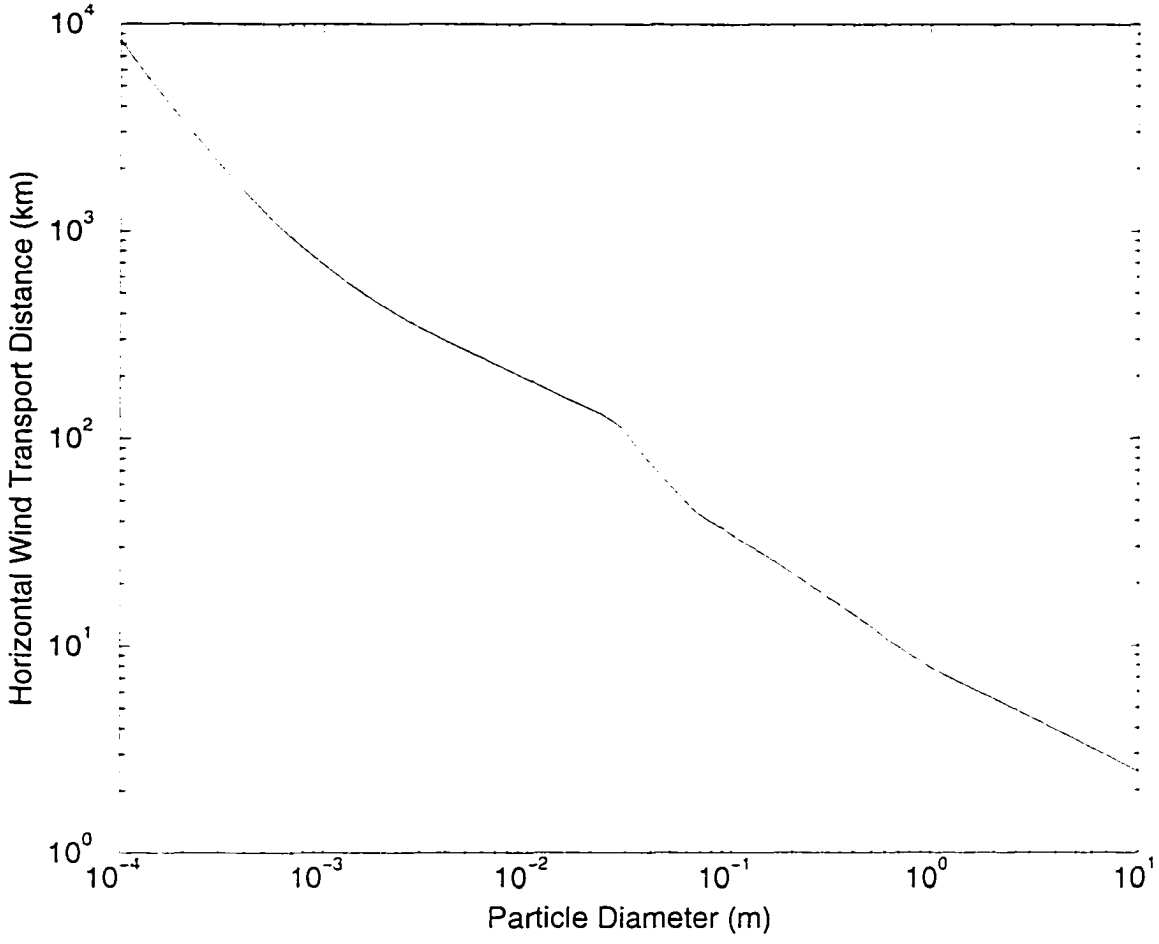

FIGURE 2: Wind transport distance versus ejecta particle diameter for particles re-entering the Venusian atmosphere. The kink in the plot is due to the "drag crisis" that Vervack and Melosh (1992) noted, as the flow of atmosphere around the particle changes from laminar to turbulent.

FIGURE 3. Anatomy of a Parabola

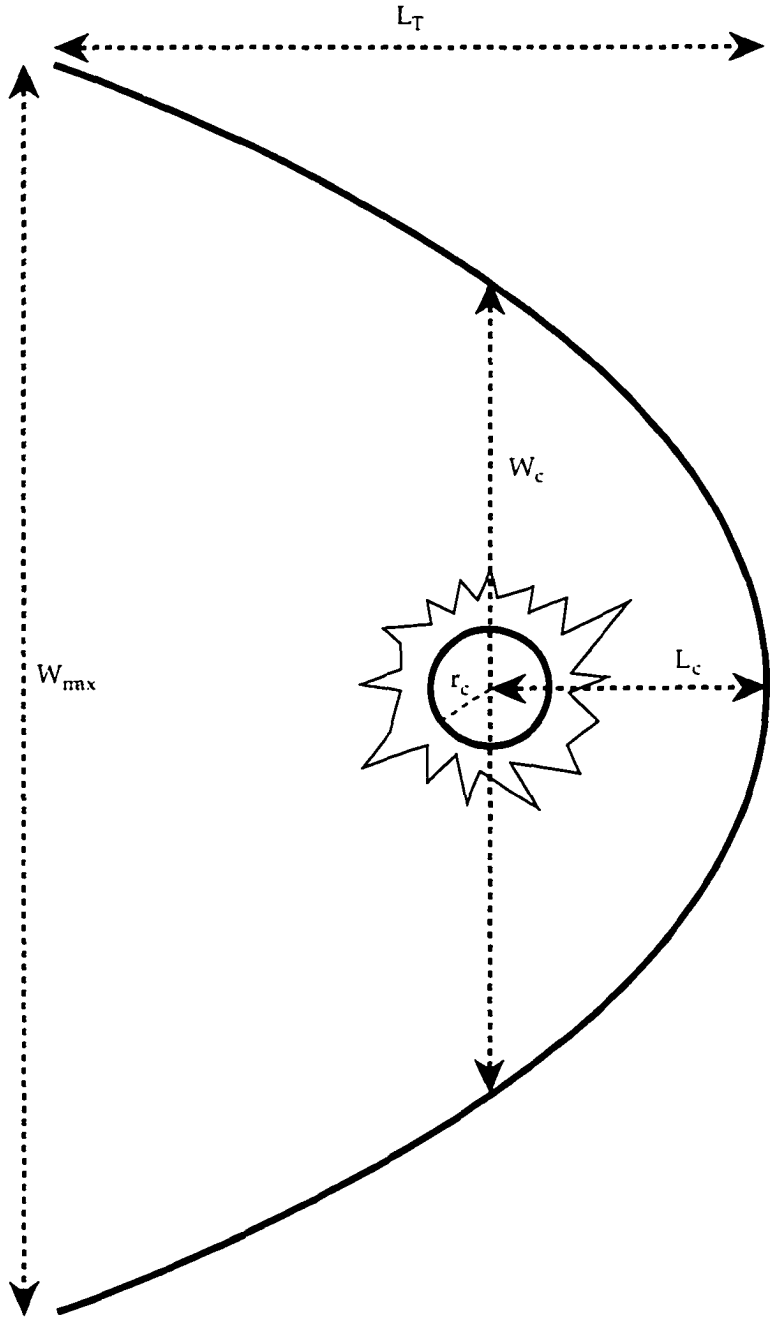

FIGURE 3: Schematic representation of a parabola and its putative source crater, showing r_c, L_c, W_c, L_T, and W_{max}.

TABLE 2. Observed Parabola Parameters (Caption)

TABLE 2: Observed parameters of Venusian ejecta parabolas. I follow the convention of Campbell et al. (1992) in classifying the deposits: "pd" indicates a dark (low backscatter cross section) parabola, "pa" indicates a parabola of the same general form as Adivar (i.e., a dark parabola with a smaller interior parabola with higher backscatter cross section), "po" indicates a so-called "open parabola," "pb" is a bright (high backscatter cross section) parabola, "pe" indicates a parabola that appears in the emissivity data, and "c" indicates a more circular deposit. Crater names, locations, and radii come from Schaber et al. (1992). Values for L_c (the distance from the center of the putative source crater to the parabola head), L_T (the total length of the parabola), and W_{max} (the width of the parabola) come from Campbell et al. (1992). Values for W_c (the width of the parabola at the source crater's central longitude) come from my measurements.

TABLE 2, Observed Parabola Parameters

	Source Crater				Observed Parabola Dimensions (km)			
Name	Lat. (°N)	Long. (°E)	r_c	Type	L_c	W_c	L_T	W_{max}
Annia Faustina	22.10	4.70	11.25	pd	85	453	630	720
Holiday	-46.75	12.85	13	pd	126	800	1180	750
Ruth	43.29	19.90	9.0	pd	77	220	900	1100
Stuart	-30.75	20.20	34.5	pd	198	795	1220	1660
unnamed	33.45	22.70	9.75	pd	86	580	960	930
Bathsheba	-15.10	49.35	18.0	pd	230	800	1530	1640
Francesca	-28.0	57.70	9.0	pd	63	280	410	410
Bassi	-18.95	64.70	16.5	pd	88	440	880	1070
Jadwiga	68.40	91.00	6.25	pd	40	110	400	590
Li Quingzhao	23.75	94.55	10.75	pd	70	400	710	756
Boulanger	-26.55	99.30	36.0	pd	270	960	1330	1680
Caldwell	23.55	112.10	22.0	pd	130	590	1290	1250
Yonge	-14.00	115.10	12.75	pd	108	440	880	970
Merit Ptah	11.30	115.65	9.25	pd	30	220	740	560
Pimiko	19.00	124.17	18.25	pd	150	510	930	1160
Phyllis	12.30	132.40	6.25	pd	77	210	390	290
Greenaway	22.95	145.00	46.0	pd	468	2000	1750	1990
Ban Zhao	17.20	146.90	21.0	pd	170	500	1120	990
Austen	-25.00	168.35	23.0	pd	240	830	990	1380
Winema	3.00	168.60	11.0	pd	72	260	240	390
Martinez	-11.65	174.70	12.5	pd	240	790	860	700
Akiko	30.65	187.10	11.75	pd	70	160	590	440
Yablochkina	48.27	195.15	31.5	pd	366	940	1260	1520
unnamed	2.32	198.25	20.0	pd	135	400	700	760
Edinger	-68.80	208.35	17.0	pd	90	250	460	410
Boleyn	24.40	219.90	34.5	pd	230	1060	940	1500
Akeley	8.00	244.40	12.25	pd	90	360	750	850
Glaspell	-58.45	269.60	13.0	pd	147	440	1300	772
Lyon	-66.55	270.50	6.75	pd	94	230	685	520
Montesori	59.45	280.25	21.75	pd	140	840	1150	1300
Cotton	70.75	300.30	23.5	pd	142	450	1300	950
Dashkova	78.30	306.20	23.75	pd	270	770	965	1220
Aurelia	20.25	331.85	15.5	pd	130	414	640	750
Magnani	58.60	337.00	13.3	pd	88	257	690	527
Comnena	1.20	343.65	9.75	pd	72	230	470	560
Carson	-24.20	344.10	20.5	pd	148	504	980	950
Audrey	23.75	348.67	7.6	pd	36	113	165	160
Adivar	8.95	76.10	15.5	pa	175	460	1020	860

TABLE 2—*continued*

unnamed	−39.10	97.10	4.0	po	50	200	400	550
Monika	72.30	122.30	13.0	po	262	560	770	455
du Chatelet	21.50	164.95	9.25	pa	135	560	720	760
Guan-Daosheng	−61.05	181.80	23.0	pa	244	515	1560	1600
Sitwell	16.68	190.35	17.25	po	110	560	760	840
Von Schuurman	−5.00	190.95	14.5	pa	115	430	720	710
Eudocia	−59.05	201.80	13.75	pa	370	820	1080	1250
Stowe	−43.20	233.00	41.0	po	460	1280	1520	1320
Adaiah	−47.30	253.35	9.5	pa	225	215	830	822
Sabin	−38.5	274.65	18.0	pa	300	1250	1200	1630
Abington	−47.75	277.80	11.25	pa	63	300	795	515
Cohn	−33.20	208.10	10.25	pb	110	400	770	830
unnamed	2.90	4.95	3.0	pe	52	220	655	767
Frank	−13.10	12.90	11.5	pe	126	493	574	890
unnamed	−40.80	151.60	6.5	pe	50	300	460	560
unnamed	66.20	177.60	2.5	pe	23	230	480	560
Rose	−35.15	248.20	7.5	pe	220	765	810	1110
unnamed	0.90	338.75	5.4	pe	38	238	705	835
unnamed	10.60	346.30	6.4	pe	90	389	690	709
Nadine	7.80	359.10	9.5	pe	102	455	1033	923
Flagstad	−54.30	18.90	20.0	c	245	280	315	280
Zenobia	−29.35	28.55	19.5	c	480	890	900	890
Ermolova	60.25	154.20	32.0	c	500	900	945	900
unnamed	17.40	170.40	19.0	c	250	650	653	670
Stanton	−23.40	199.90	55.0	c	1030	2150	1900	2100
Mumtaz Mahal	30.25	228.35	19.5	c	330	860	690	860
Hayasi	53.85	243.65	23.5	c	500	770	1000	730
Galina	47.55	307.10	9.0	c	270	300	470	345
Lind	50.25	355.00	14.0	c	195	215	325	240

TABLE 2: (Caption on page 22)

CHAPTER 3

Results

Table 3 shows the best values of α, d_c, and δ for each of the parabolas: I also report the mean thickness T_{mean} (i.e. the total volume divided by the total area) of the theoretically-modeled parabolas. I fit most values of L_c to within ~10%. I fit W_c to within ~20% for the majority of craters with $r_c > 9.5$ km. W_{max} and L_T were generally fit to within ~50%. W_{max} and L_T describe the more diffuse regions of the parabola and thus contain more observational uncertainty than W_c or L_c, so the 50% uncertainty may be partially due to observational measurement error. The systematically poor fits in these dimensions, however, suggest that the model may not account for every aspect of the emplacement of an ejecta parabola. Observational parameters W_c and L_c describe the portion of the parabola that is most sharply defined and therefore most accurately known, which helps explain the good fit of the theoretical model. In addition, this region of the parabola (the head) contains the most material as well as the largest particles, which fall closer to the source crater than smaller particles (Eq. 1). Post-emplacement modification processes that affect the parabolas are therefore likely to require longer timescales to modify the shape of the head than the tail.

I successfully matched 32 of the 58 strictly parabolic features and 1 of the 9 circular features. I define a "successful" fit as one in which the L_c and W_c dimensions are each fit to within 20%. In addition, the shape of the modeled deposit must agree well with the observed parabola. For example, the unnamed feature located at –39.10°N, 97.10°E, seems to be a successful fit according to Table 3 (8% error in L_c, –6% error in W_c). Examination of the modeled deposit (Figure 4), however, reveals the union of a very narrow crescent and a circle instead of a parabola at the $\delta = 1$ cm contour. Thus, the

model fails for this feature, which has a crater radius of $r_c = 4.0$ km.

17 of the 58 parabolas have source craters with $r_c \leq 9.5$ km. In general, I was unable to model this population of parabolas with this method, since the source craters of these parabolas have radii on the same order as (or less than) the transition radius that Vervack and Melosh (1992) calculated. The slightly larger r_t defined by this population (9.5 km compared to the 8 km calculated radius) probably reflects the role of aero-braking that Vervack and Melosh explicitly neglected (Section 2.1). If I discard the population of parabolas outside the model's requirements, I have successfully matched 27 out of 41 parabolas, approximately 65% of the applicable population. (This number includes those parabolas that I could model only with $\delta > 1$ cm.) Figure 1b shows the best model fit to Bassi. Figure 5a shows an example of a parabola with a putative source crater (DuChatelet, $r_c = 9.25$ km) that has $r_c < r_t$. Figure 5b shows the best model fit to DuChatelet; the model fails for DuChatelet, since $r_c < r_t$.

One noteworthy detail of Table 3is the extremely poor "best fit" to the L_c dimension of the features that Campbell et al. (1992) classify as circular deposits. While the W_c, L_r, and W_{max} fits tend to be quite good (with a few exceptions, namely Stanton and Mumtaz Mahal), the L_c fits tend to be extremely low. The model underpredicts this dimension by ~50%. Occam's Razor suggests that the processes that formed these large circular deposits should not be radically different from the processes that formed the parabolas. The final shape of the modeled deposit depends, in part, on the details of how the particles fall within the atmosphere (phase 4 of the model) as well as the partitioning of kinetic energy during the initial stage of the particles' ballistic trajectory (phase 2 and Eq. 1). Changes in these stages of the model would tend to alter the shape of the final deposit. I leave further discussion and investigation of these details to future work.

An additional point of interest comes from the observation that one misfit parabola,

Greenaway, corresponds to the largest crater (r_c = 46 km) on Venus to exhibit a strictly parabolic deposit. An additional misfit deposit, Stanton, corresponds to the largest crater (r_c = 55 km) to exhibit a circular feature. During their fall to the surface, ejecta particles from craters of these large sizes may be close enough to each other to introduce significant inter-particle forces, violating the assumptions of the model. In addition, for ejecta from large craters, the curvature of the planet may become important. I successfully fit the parabolas around the craters Stuart and Stowe (34.5 km and 41 km radius, respectively), however, suggesting that the transition radius to this new, hypothetical domain (where inter-particle forces and planetary curvature become important) is between 41 km and 46 km.

The existence of a second large crater (Marie Celeste, at 23.45° N, 140.2°E, r_c = 47.5 km) within the Greenaway parabola may further complicate attempts to model that feature. If Marie Celeste is relatively young, it should also exhibit a parabola, since we expect all Venusian craters with $r_c \geq r_t$ to produce parabolas. If such a parabola exists around Marie Celeste, then this hypothetical parabola would lie within the region currently attributed entirely to Greenaway: Greenaway may actually be the union of two parabolas. It is impossible to estimate adequately Marie Celeste's age relative to Greenaway (and therefore to determine whether Marie Celeste should exhibit a parabola or not) by observing the crater floor's backscatter cross section (Chapter 1). While the crater is dark-floored, this darkening may be due to the fallout of the Greenaway ejecta rather than to age.

In Figure 6, I plot α versus r_c for the 41 strictly parabolic features with source crater r_c > 9.5 km. α is very tightly constrained and remains approximately constant over the wide range of crater radii modeled. The average value for α is 2.65 ± 0.05.

I plot the relationship between d_c and r_c in Figure 7. The best least-squares fit to this

relationship is a power-law function:

$$d_c = 2400 r_c^{-1.62 \pm 0.28}. \tag{2}$$

where d_c is in meters and r_c in kilometers. The coefficient in Eq. 2 has a 1-σ range of $10^{3.39 \pm 0.35}$, i.e. from 1100 to 5500, or about a factor of 2. Note that the reference size decreases with increasing crater size. Extrapolating the particle size back to the crater rim ($r = r_c$) suggests that large craters will have smaller ejecta near the rim than smaller craters. This result is contrary to observations of blocks on lunar crater rims (e.g. Moore, 1971); however, my work focuses on the distal portion of a crater's ejecta, so the extrapolation from our results back to the crater rim may not be meaningful (Chapter 2).

Campbell et al. (1992) constrain the mean thickness T_{mean} of the observed parabolas by modeling the reduction of backscatter cross section across plains units that the parabola material has partially covered. Their analysis is consistent with thicknesses of a few centimeters to a few meters. My results agree with their estimates: the best fit to Cohn (r_c = 10.25 km) has T_{mean} = 1 cm, and the best fit to Stowe (r_c = 41.0 km) has T_{mean} = 137 cm. Cohn and Stowe represent the extremes of model parabola mean thicknesses. For a typical model parabola, 2 cm < T_{mean} < 20 cm; larger craters produce more material of a given size and therefore thicker parabolas.

Finally, I matched the model to most of the parabolas assuming δ = 1 cm; I could only fit the remaining few, however, with higher values of δ. The larger values of δ for these parabolas may be an age effect; I explore the implications of this observation in the next chapter.

TABLE 3, Modeled Parabola Parameters (Caption)

TABLE 3: Best-fit model parameters and dimensions for the Venusian ejecta parabolas. I show the percent-error between the best model and the observed deposit in each case; the percent-error is calculated as (model dimension – observed dimension)/observed dimension. A bullet ("•") beside a parabola's name indicates that I consider it to be a successful fit; parabolas with source crater $r_c \leq 9.5$ km are not included with the successes, as discussed in Chapter 3. r_c is the crater radius, α and d_c are parameters for Eq.1, δ is the minimum detectable thickness, and T_{mean} is the mean thickness of the deposit. L_c, W_c, L_T, and W_{max} are defined in the caption for Table 2.

TABLE 3. Modeled Parabola Parameters

	Model Parameters				Best-Fit Model Dimensions				
Name	r_c (km)	α	d_c	δ	L_c	W_c	L_T	W_{max}	T_{mean}
•Annia Faustina	11.25	2.68	38	1	8%	-13%	-20%	-15%	2
Holiday	13	2.62	37	1	5%	-31%	-52%	-15%	3
Ruth	9.0	2.67	55	1	1%	35%	-57%	-57%	4
•Stuart	34.5	2.67	3.75	1	-1%	9%	-22%	-21%	8
unnamed	9.75	2.65	57	1	9%	-30%	-57%	-48%	5
•Bathsheba	18.0	2.63	26	1	6%	15%	-45%	-42%	7
Francesca	9.0	2.47	27	1	11%	-12%	-7%	0%	5
•Bassi	16.5	2.65	12	1	7%	-1%	-25%	-16%	7
Jadwiga	6.25	2.57	46	1	5%	38%	-48%	-44%	1
•Li Quingzhao	10.75	2.63	31	1	17%	-16%	-34%	-22%	2
•Boulanger	36.0	2.64	4.5	1	1%	14%	-22%	-24%	88
•Caldwell	22.0	2.65	8	1	0%	8%	-35%	-10%	20
•Yonge	12.75	2.75	39	1	-3%	5%	-39%	-26%	3
Merit Ptah	9.25	2.64	12	1	7%	-41%	-44%	-15%	5
Pimiko	18.25	2.64	17	1	-1%	36%	-21%	-18%	7
Phyllis	6.25	2.65	170	1	6%	20%	-38%	-2%	2
Greenaway	46.0	2.59	20	1	-14%	-43%	-43%	-43%	221
Ban Zhao	21.0	2.58	10	1	5%	53%	-17%	7%	14
•Austen	23.0	2.66	14	1	1%	20%	1%	-11%	17
•Winema	11.0	2.67	33	3	8%	0%	21%	-1%	4
•Martinez	12.5	2.66	185	1	2%	-20%	-33%	-9%	3
Akiko	11.75	2.65	20	1	3%	50%	-11%	10%	4
•Yablochkina	31.5	2.65	10	1	1%	16%	-12%	-25%	56
unnamed	20.0	2.64	12.5	3	2%	47%	-7%	0%	15
•Edinger	17.0	2.64	18	50	11%	0%	-46%	-28%	22
•Boleyn	34.5	2.63	4.25	1	5%	-5%	6%	-16%	78
•Akeley	12.25	2.67	27	1	-2%	6%	-28%	-18%	3
Glaspell	13.0	2.60	50	1	17%	40%	-52%	-15%	3
Lyon	6.75	2.50	120	1	6%	37%	-60%	-37%	2
•Montesori	21.75	2.67	10	1	9%	-14%	-23%	-9%	17
•Cotton	23.5	2.70	12	23	3%	1%	-68%	-49%	22
•Dashkova	23.75	2.65	18	4	-3%	-2%	-19%	-35%	19
Aurelia	15.5	2.62	55	1	5%	29%	-17%	-23%	2
•Magnani	13.3	2.70	18	1	-11%	7%	-14%	9%	5
•Comnena	9.75	2.78	50	1	0%	4%	-12%	-12%	5
Carson	20.5	2.60	9.5	1	0%	35%	-10%	7%	15
Audrey	7.6	2.74	30	1	-5%	17%	22%	8%	9

TABLE 3—*continued*

•Adivar	15.5	2.72	52	3	2%	17%	-53%	-34%	5
unnamed	4.0	2.49	205	1	8%	-6%	-63%	-62%	< 1
•Monika	13.0	2.60	220	1	-17%	-11%	-35%	10%	8
du Chatelet	9.25	2.70	160	1	5%	-25%	-49%	-42%	4
Guan-Daosheng	23.0	2.54	45	1	-4%	31%	-54%	-55%	2
•Sitwell	17.25	2.65	15	1	7%	0%	-11%	-2%	9
Von Schuurman	14.5	2.67	27	1	3%	21%	-15%	0%	5
•Eudocia	13.75	2.60	340	1	-3%	-14%	-30%	-43%	2
•Stowe	41.0	2.66	10.5	1	-13%	-15%	-28%	-15%	137
Adaiah	9.5	2.66	50	3	-63%	53%	-51%	-40%	4
Sabin	18.0	2.55	29	1	3%	-31%	-25%	-45%	6
Abington	11.25	2.64	26	1	24%	-2%	-38%	7%	3
•Cohn	10.25	2.79	90	1	-3%	12%	-40%	-36%	1
unnamed	3.0	2.56	850	1	-11%	-52%	-83%	-85%	< 1
•Frank	11.5	2.65	55	1	3%	7%	-9%	-36%	2
unnamed	6.5	2.61	76	1	16%	-33%	-53%	-43%	2
unnamed	2.5	2.60	400	1	13%	-100%	-95%	-84%	< 1
Rose	7.5	2.62	370	1	-25%	-59%	-57%	-71%	2
unnamed	5.4	2.71	125	1	26%	-29%	-74%	-77%	< 1
unnamed	6.4	2.55	140	1	2%	-23%	-63%	-56%	1
Nadine	9.5	2.56	54	1	2%	-10%	-66%	-52%	4
Flagstad	20.0	2.60	15	1	-51%	7%	2%	10%	77
Zenobia	19.5	2.52	59	1	-30%	-2%	-11%	0%	10
Ermolova	32.0	2.65	12	1	-41%	0%	3%	10%	66
•unnamed	19.0	2.66	67	3	2%	5%	-3%	6%	15
Stanton	55.0	2.43	1	1	-70%	-44%	-44%	-41%	414
Mumtaz Mahal	19.5	2.57	140	1	-10%	-23%	-4%	-23%	21
Hayasi	23.5	2.54	35	1	-40%	0%	-18%	10%	29
Galina	9.0	2.69	90	1	-63%	1%	-31%	9%	7
Lind	14.0	2.62	10	1	-66%	0%	0%	10%	12

TABLE 3: (Caption on page 29)

FIGURE 4. Unnamed Parabola at –39.10°N, 97.10°E

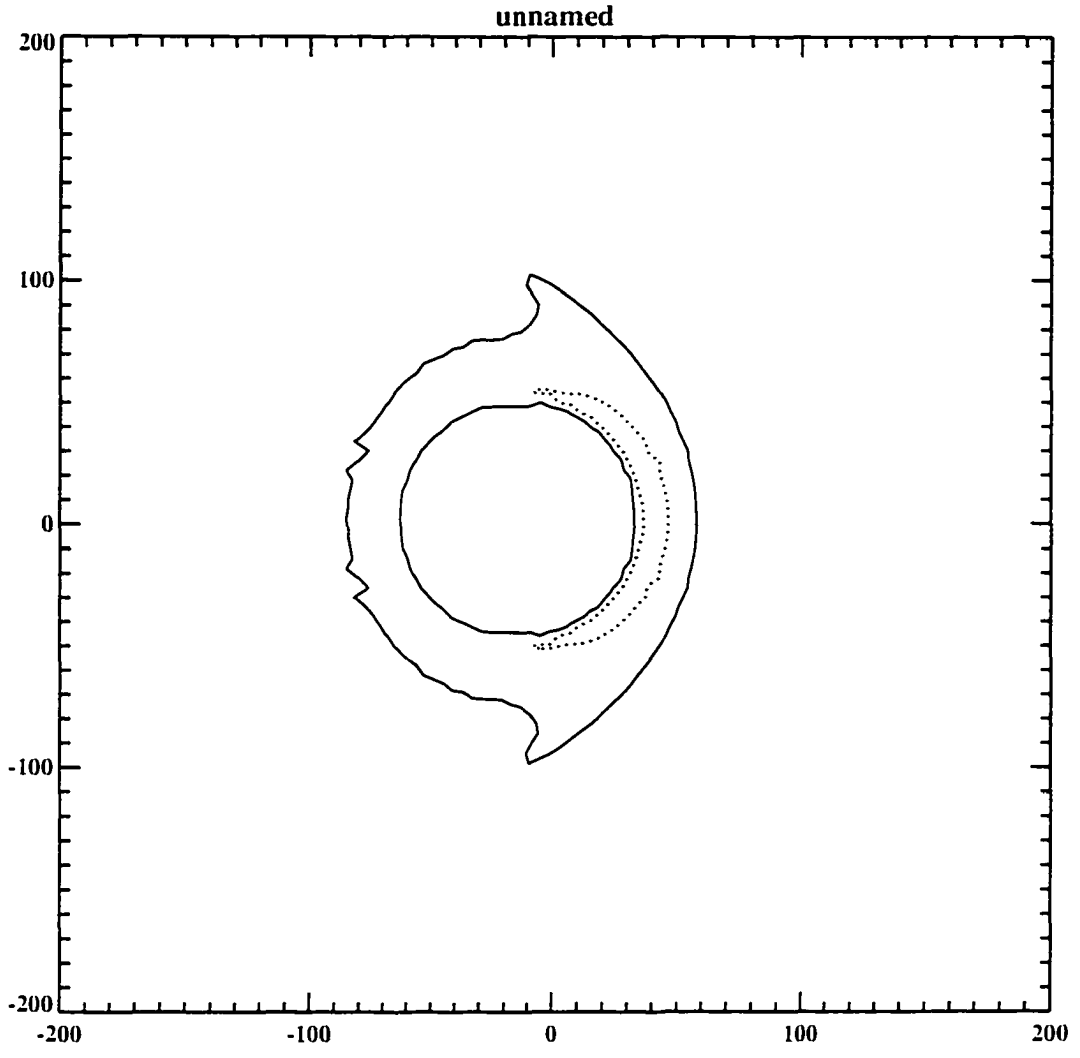

FIGURE 4: The thickness contours for the unnamed feature located at –39.10°N, 97.10°E (r_c = 4.0 km), showing that the deposit is not a successful fit, despite the good results in Table 3. Contours are shown for 1 cm (solid line) and 3 cm (dashed line). The center of the crater is located at the origin of the plot. Note the change in scale between this figure and Figure 1b. Distances are in km.

FIGURE 5a, DuChatelet Parabola

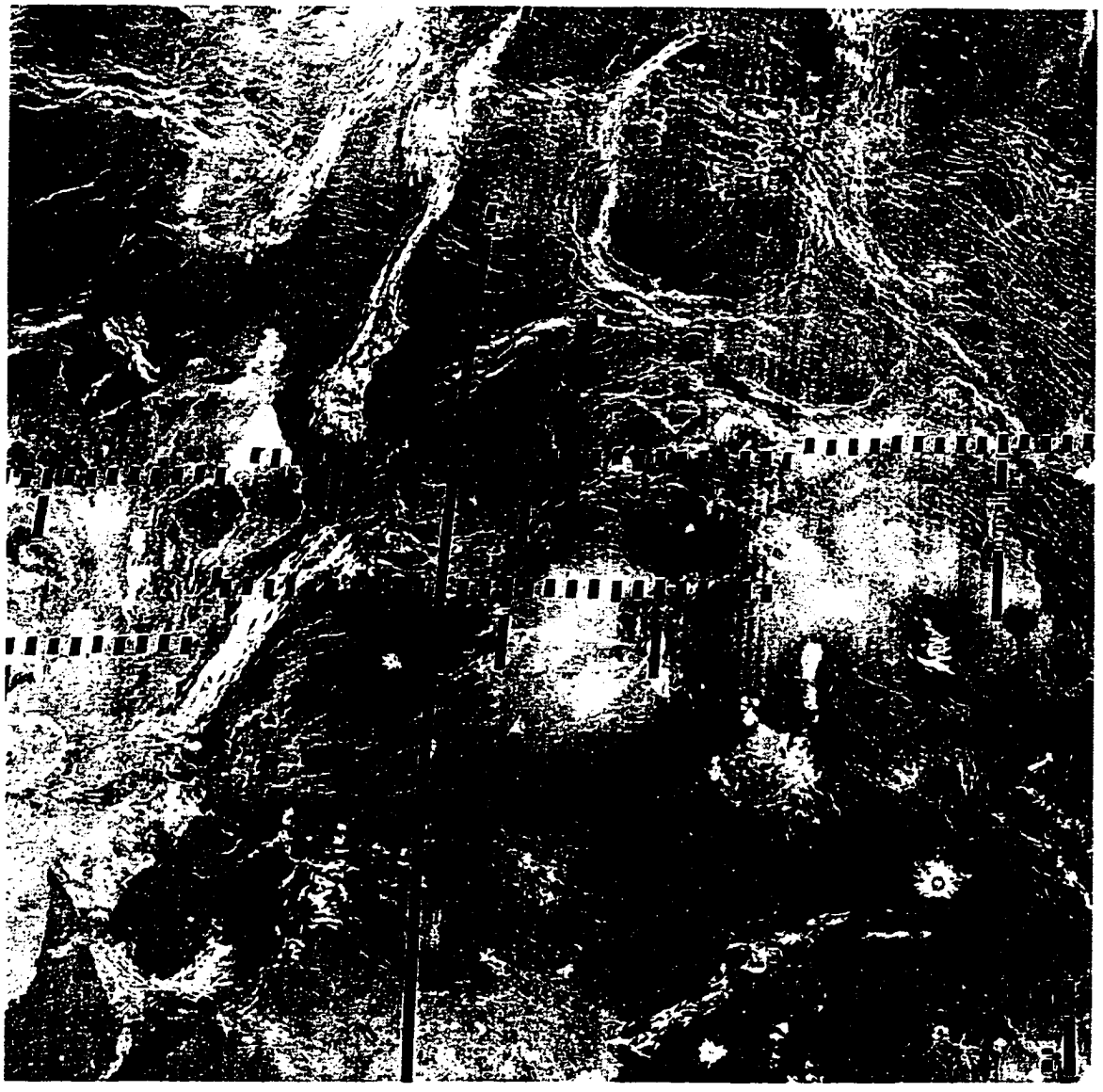

FIGURE 5: (a) The ejecta parabola around the crater DuChatelet, located at 21.5°N, 165.0°E, rc = 9.25 km. Note that for DuChatelet, $r_c < r_r$. The image is approximately 1800 km across. (Image from C2-MIDR.00N183;1.)

FIGURE 5b, DuChatelet Parabola (Modeled)

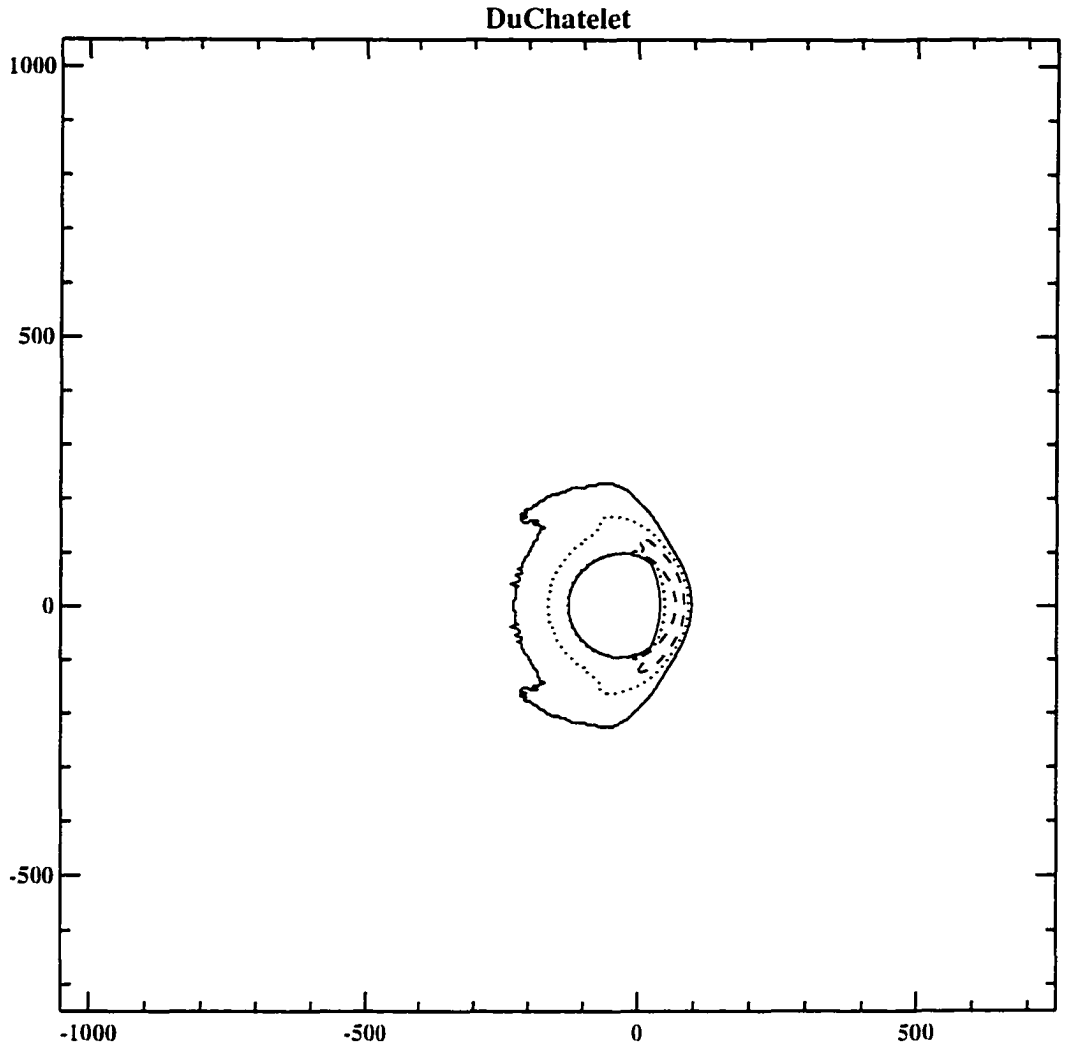

FIGURE 5: (b) Thickness contours for the best fit model to DuChatelet, using $\alpha = 2.65$, $d_c = 65$ m, and $\delta = 1$ cm. Contours are show for 1 cm (solid line), 3 cm (short dash), and 10 cm (long dash). Higher contours were omitted for clarity. Distances are in km. The plot is at the same scale as (a), and the crater DuChatelet is located at the origin of the plot. The origin of the plot matches the center of DuChatelet in Figure 5a.

FIGURE 6, α *vs.* r_c

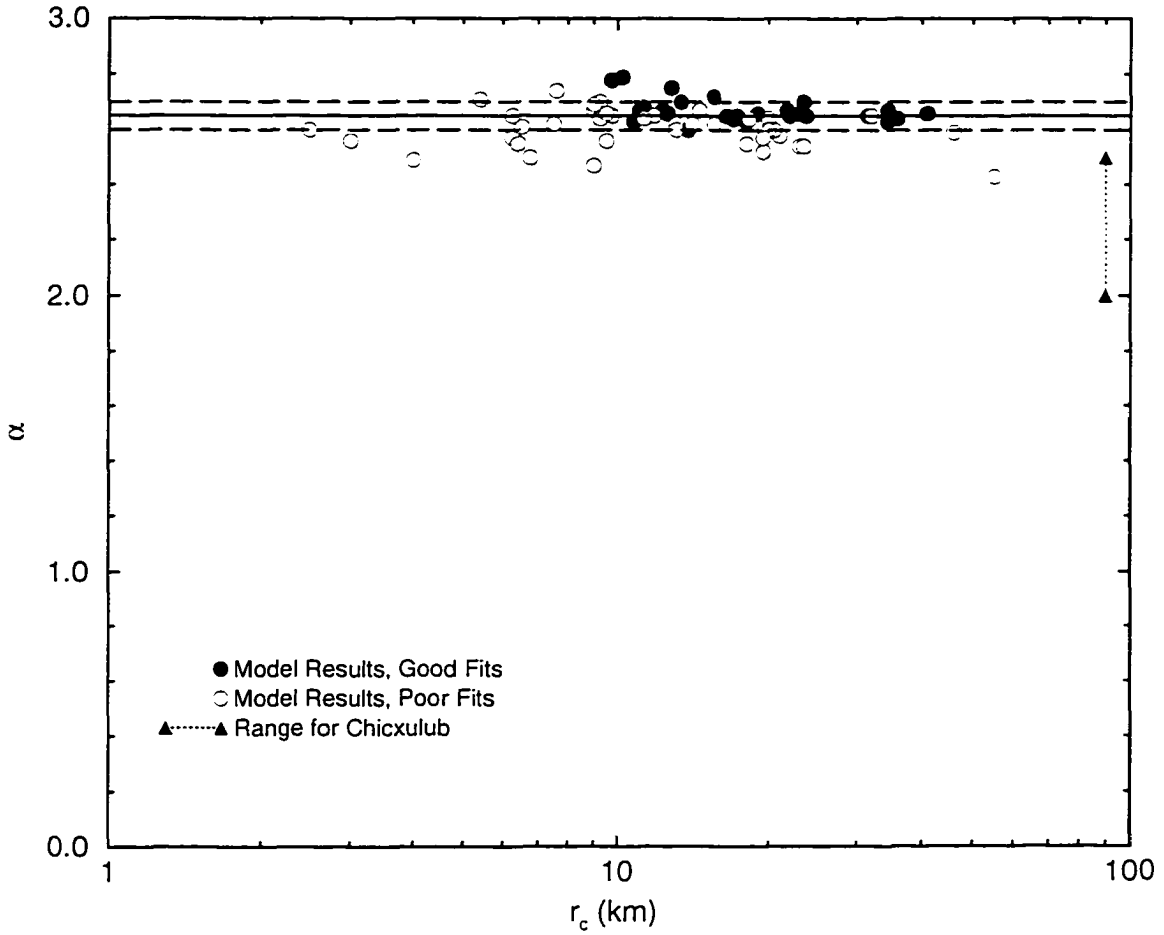

FIGURE 6: Plot of α versus r_c. The range of α for ejecta from the Terrestrial impact structure off the coast of Chicxulub, Mexico is shown for comparison. The dashed lines indicate the standard deviation in the average value for α.

FIGURE 7, d_c vs. r_c

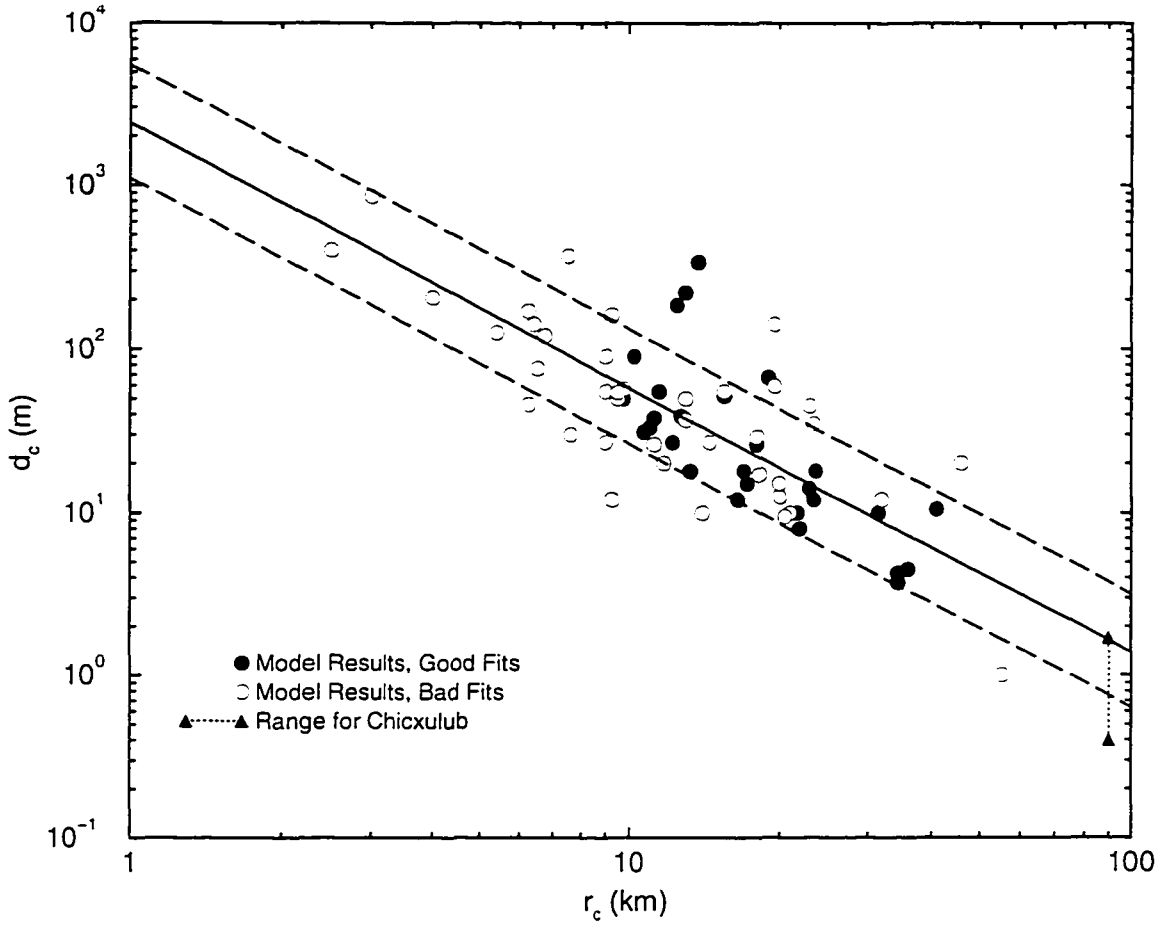

FIGURE 7: Plot of d_c versus r_c. The range for ejecta from Chicxulub is shown for comparison. The dashed lines indicate the 1-σ error in intercept of the best fit curve to the data.

CHAPTER 4

Discussion

This investigation has identified three important implications: (1) Observational evidence supports the transition size calculation of Vervack and Melosh (1992) (with only slight modifications) and thus reinforces their model, (2) we can apply this model of the scattering of distal ejecta to Terrestrial impacts, including the crater Chicxulub, and (3) the role of the minimum thickness δ may be significant in determining the relative ages of the parabolas. I consider each of these topics below.

4.1. Source Crater Transition Radius

I noted in the previous chapter that fifteen of the parabolas that I cannot reproduce using this model have source craters of $r_c \leq 9.5$ km. This result supports the transition size calculation of Vervack and Melosh (1992), who predicted that the actual size would be slightly larger than their result ($r_t = 8$ km) due to their neglect of aero-braking. I set an upper limit for r_t of 9.5 km for Venusian atmospheric and surface conditions.

Interestingly, each of the eight features identified as emissivity parabolas (i.e. parabolas that appear only in the Magellan emissivity data-set) by Campbell et al. (1992) (in their Table II) has a source crater of $r_c < r_t$, with the exception of crater Frank, with $r_c = 11.5$ km (as measured by Schaber et al. [1992]). Thus, a different process than the one that Vervack and Melosh describe may be responsible for the formation of the emissivity parabolas. Frank is an apparent anomaly; it is an emissivity parabola with source crater $r_c > r_t$, but I can reproduce it with the model of Vervack and Melosh (1992), as can I several SAR parabolas with $r_t < r_c < r_{Frank}$ (e.g. Cohn, Comnena, and Winema). Thus, the process that forms emissivity parabolas may be different than the process that forms

parabolas with source craters smaller than the transition radius. The fact that r_{Frank} (the apparent upper-bound of emissivity parabola formation) agrees well with the Vervack-Melosh transition radius may be a coincidence.

4.2. Agreement with Chicxulub and Extension to Non-Venusian Craters

Vervack and Melosh (1992) report the estimated parameters α and d_c for the distal ejecta from the Terrestrial crater Chicxulub. (r_c = 90 km, α is in the range from 2.0 to 2.5, and d_c is in the 1.4 to 1.7 m range.) I plot these parameters in Figures 6 and 7 for comparison with the model results. They agree quite well with my results, suggesting that the distribution model for distal ejecta (Eq. 1 and Eq. 2) may be equally valid for non-Venusian craters.

The agreement with the Chicxulub data suggests that we can extend the model to other planets that have atmospheres, particularly Titan but perhaps Mars as well. Determining the parameters for Mars requires extensive *in situ* exploration, as global climate patterns would tend to erode impact ejecta deposits, much as they do on Earth. For Titan, however, the radar mapper aboard Cassini may provide an opportunity similar to that of Venus (Lorenz et al., 1996).

4.3. The Role of Minimum Thickness δ

Eight parabolas around craters with radii in the range of 9.5 to 24 km can only be fit by the model of Vervack and Melosh (1992) if the ejecta thickness contour, δ, is larger than 1 cm at the limit of discernibility. Aside from requiring a larger δ, there is nothing special about these craters: 45% of all Venusian craters (Schaber et al., 1992) and 65% of all craters with parabolas have radii between 9.5 km and 24 km. These eight parabolas are scattered over Venus in roughly the same spatial distribution as the remainder; they

are not localized in one particular region. Assuming, then, that these eight parabolas were formed under similar conditions, in similar environments, and by the same process as the remaining 59 features, we would expect them to have originally possessed the same δ as well. I propose that the observed discrepancy in d is caused by the erosion of material from the ejecta deposits of these craters and thus indicates that these parabolas are older and more degraded than the rest. This erosion is probably eolian, caused by the gradual removal of sand-size grains by saltation and dust-size material in suspension. The identification by Greeley, et al. (1992) of two fields of apparent sand dunes in the Magellan data suggests that aeolian process are currently active on the surface of Venus.

In the final phases of the formation of a parabola, the accumulating ejecta builds up a graded deposit, such that the larger particles (about 1 to 5 cm for craters with radii in the range of 10 to 40 km) are closer to the source crater and at the bottom of the pile (qualitatively similar to the airfall deposits of volcanic ash on Earth). The smallest particles in a parabola (about 200 to 1000 μm) are the most distant and on top, because they travel greater distances on their ballistic trajectories than larger particles (Eq. 1) and settle more slowly once they have reached terminal velocity (Section 2.1). As surface Venusian winds selectively remove these fine top layers of ejecta debris, the overall area of the parabola decreases. The remaining, coarser, deposits are distributed in a pattern that reflects a larger thickness contour than the original $\delta = 1$ cm, as we observe for these eight parabolas.

If this interpretation is correct, the relatively small number of degraded parabolas, 8, compared to 59 undegraded parabolas also indicates that the removal process, once it begins, acts swiftly to erase the entire parabola. In this sense, parabolas are similar to terrestrial cinder cones which stand unscarred by fluvial channels for long periods of time due to the high infiltration capacity of the loose, highly porous cinders. However, once

soil begins to develop on these cones and runoff begins, their lack of resistance to shear forces makes them disappear in a geologic blink of time. Clearly, fluvial processes are not implicated in Venusian parabola removal, but some weathering-related threshold process must be inferred to explain the small proportion of degraded parabolas. From this proportion alone, 8/59 degraded parabolas, it appears that the mean interval between the beginning of observable degradation and complete removal is about 0.14 ± 0.05 of the mean lifetime of the parabolas themselves.

Arvidson et al. (1992) first estimated the mean time to remove a parabola as ~60 Myr, assuming that all Venusian craters originally possessed one. My present observations allow me to refine this estimate somewhat. The parabola formation model of Vervack and Melosh suggests that nearly all impact craters should form parabolic deposits; even craters with $r_c < r_t$ have parabolas, down to $r_c = 2.5$ km (an unnamed crater at 66.2° N, 177.6° E), the smallest crater to exhibit a parabola. It is highly probable, then, that a parabolic deposit accompanies the formation of any impact crater on Venus, possibly with a lower limit of $r_c = 2.5$ km. This supposition implies that aeolian processes eventually remove (or blanket) all of the material in a parabola, leaving only the source crater to scatter radar energy. Hence, the Venusian craters that do not have parabolas are part of an older crater population.

Schaber et al. (1992) identified 842 impact craters over 89% of the surface of Venus. Of these craters, 17 have $r_c \leq 2.5$ km, leaving 825 craters that might have formed with accompanying parabolas. Normalizing over the entire surface of the planet, there may be ~930 such craters. If we assume that the surface of Venus is 500 ± 200 million years old (Schaber et al., 1992) and that the rate of impact cratering has been steady over this period (as Schaber et al. and other researchers have suggested, based on impact crater populations), then the mean time to erode a Venusian parabola is 35 ± 15 million years;

larger parabolas may take longer to erode than smaller ones. We expect, therefore, that the mean age of the Venusian parabolas is less than 35 ± 15 million years, with most of the removal occurring during the last ~14% of their lifespans.

Parabolas may be the principal source of "sand" size particles on the surface of Venus (i.e. particles that are in the correct size range to move predominantly by saltation, 60-2000 μm on Venus (Greeley et al. 1992) under present atmospheric conditions). Using the fits to the ejecta particle size distribution for a given crater size, Melosh and Schaller (1996) employ the McGetchin et al. (1973) estimate of ejecta blanket thickness vs. range to give the ejecta volume and my relation between mean particle size and range to give the radius limits between which sand size ejecta occur. They integrate to find the total volume of sand-size material produced by this crater.

Supposing that all Venusian impact craters larger than 2.5 km in radius produce ejecta deposits, They next integrate over the total population of craters to determine the total volume of sand-size material available. From Eq. 2, it is clear that large craters dominate the production of fine material, so the choice of the exact lower limit of crater size does not change the calculation much. Melosh and Schaller (1996) show that the total volume of sand-size material produced by Venusian impact cratering is 3.5×10^4 km^3, more than sufficient (by a factor of 10) to account for the dune fields that Greeley et al. (1992) detected. It thus appears that all of the loose sand-sized material on the surface of Venus could have been derived from impact ejecta in the form of eroded parabola material.

CHAPTER 5

Conclusions

This work supports the model of parabola formation that Vervack and Melosh (1992) have proposed: it is in good agreement with the observational results of Campbell et al. (1992). I successfully modeled 65% of the parabolas that fall within the specified physical domain of the model. Two notable exceptions are Greenaway and Stanton, which as the largest craters involved, may establish an upper boundary to the applicable crater size domain. Complicating the issue somewhat is the observation that Greenaway may have been superposed by another parabola.

I have determined a quantitative law that describes the distribution of fine, distal ejecta over a planetary surface. At a distance r from the center of an impact crater on Venus of radius r_c, the mean diameter d of the impact ejecta (neglecting the effects of wind-transport) is given by

$$\left.\begin{aligned} d &= d_c\left(\frac{r_c}{r}\right)^{\alpha} \\ \alpha &= 2.65 \pm 0.05 \\ d_c &= 2400 r_c^{-1.62 \pm 0.28} \end{aligned}\right\} \qquad (3)$$

where r_c and r are in kilometers, and d and d_c are in meters.

My modeling of the Venusian parabolas has resulted in several implications for the formation of parabolas on Venus and the distribution of fine, distal impact crater ejecta over a planetary surface: I have confirmed and improved the Vervack-Melosh transition

radius calculation with the observed Venusian parabolas. I have shown that results for the Venusian parabolas agree quite well with the Eq. 1 parameters for the Terrestrial impact crater Chicxulub; this result suggests that the distal ejecta distribution laws empirically derived for Venus might be applicable to other planetary bodies. Finally, I have presented a method for determining which parabolas are most heavily eroded and therefore older. Parabolas may be a significant source of the fine-grained material that observed dune fields imply.

REFERENCES

Arvidson, R. E., R. Greeley, M. C. Malin, R. S. Saunders, N. Izenberg, J. J. Plaut, E. R. Stofan, and M. K. Shepard 1992. Surface modification of Venus as inferred from Magellan observations of plains. J. Geophys. Res. 97, 13,303-13,317.

Campbell, D. B., N. J. S. Stacy, W. I. Newman, R. E. Arvidson, E. M. Jones, G. S. Musser, A. Y. Roper, and C. Schaller 1992. Magellan observations of extended impact crater related features on the surface of Venus. J. Geophys. Res. 97, 16,249-16,277.

Glass, B. P. and J. E. Pizzuto 1994. Geographic variation in Australasian microtektite concentrations: implications concerning the location and size of the source crater. J. Geophys, Res. 99, 19,075-19,081.

Greeley, R., R. E. Arvidson, C. Elachi, M. A. Geringer, J. J. Plaut, R. S. Saunders, G. Schubert, E. R. Stofan, E. J. P. Thouvenot, S. D. Wall, and C. M. Weitz 1992. Aeolian features on Venus: Preliminary Magellan results. J. Geophys. Res. 97, 13,319-13,345.

Lorenz, R. D. And H. J. Melosh 1996. Parabolic ejecta features on Titan? Probably not. Lunar and Planet. Sci. XXVII, 775-776.

McGetchin, T. R., M. Settle, and J. W. Head 1973. Radial thickness variation in impact crater ejecta: implications for lunar basin deposits. Earth Planet. Sci. Lett. 20, 226-236.

Melosh, H. J. and C. J. Schaller 1996. The abundance of fine-grained impact ejecta on Venus. Lunar and Planet. Sci. XXVII, 861-862.

Moore, H. J. 1971. Large blocks around lunar craters. In Analysis of Apollo 10 photography and visual observations, pp. 26-27. nasa SP-232, Washington, DC.

Schaber, G. G., R. G. Strom, H. J. Moore, L. A. Sonderblom, R. L. Kirk, D. J. Chadwick, D. D. Dawson, L. R. Gaddis, J. M. Boyce, and Joel Russell 1992. Geology and distribution of impact craters on Venus: What are they telling us? J. Geophys. Res. 97, 13,257-13,301.

Seiff, A., J. T. Schofield, A. J. Kliore, F. W. Taylor, S. S. Limaye, H. E. Revercomb, L. A. Sromovsky, V. V. Kerzhanovich, V. I. Moroz, and M. Ya. Marov 1985. Models of the structure of the atmosphere of Venus from the surface to 100 kilometers altitude.

Adv. Space Res. 5, 3-58.

Vervack, R. J. Jr. And H. J. Melosh 1992. Wind interaction with falling ejecta: origin of the parabolic features on Venus. Geophys. Res. Lett. 19, 525-528.

IMAGE EVALUATION TEST TARGET (QA-3)

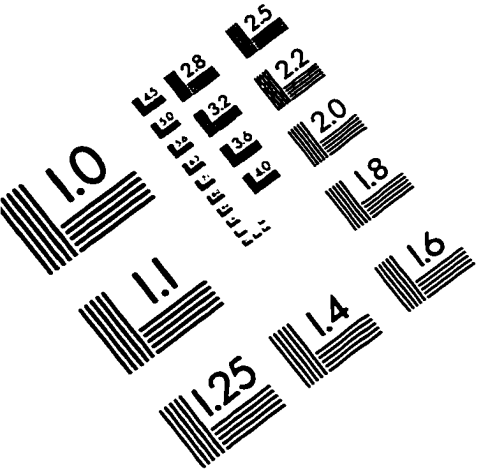

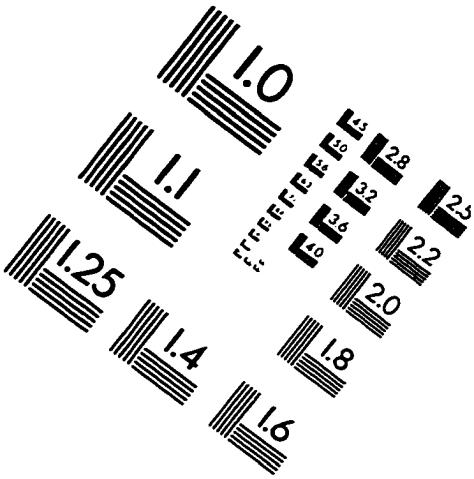

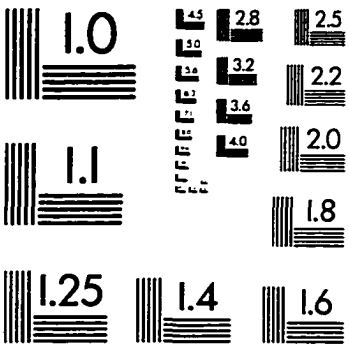

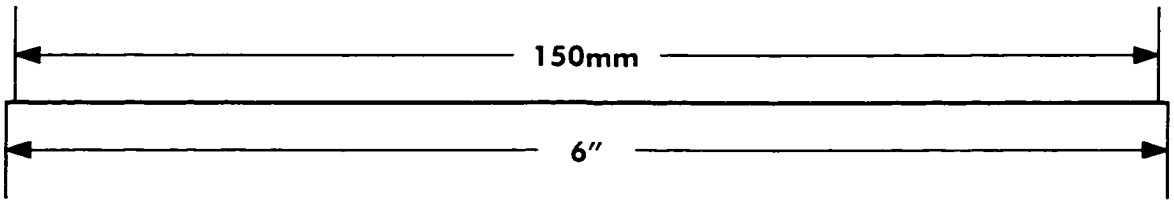

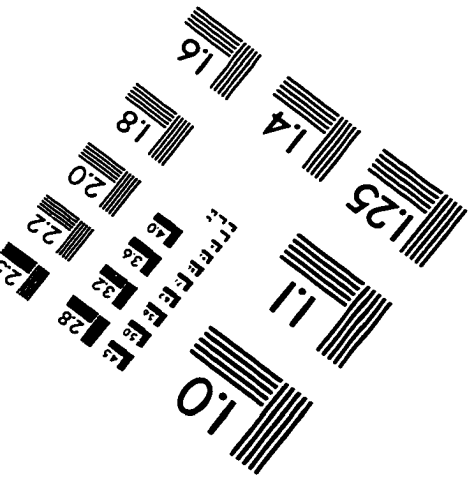

APPLIED IMAGE, Inc
1653 East Main Street
Rochester, NY 14609 USA
Phone: 716/482-0300
Fax: 716/288-5989
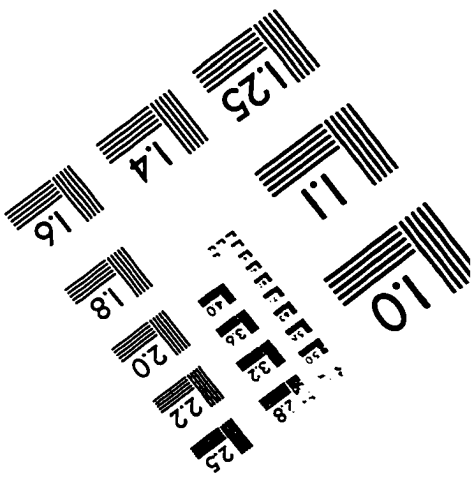
© 1993, Applied Image, Inc., All Rights Reserved